

Local Bandwidth Estimation via Mixture of Gaussian Processes

Danny Panknin
Shinichi Nakajima
Thanh Binh Bui
Klaus-Robert Müller*
Marchstraße 23, MAR 4-1
10587 Berlin, Germany

DANNY.PANKNIN@TU-BERLIN.DE
NAKAJIMA@TU-BERLIN.DE
BUI@TU-BERLIN.DE
KLAUS-ROBERT.MUELLER@TU-BERLIN.DE

Editor: TBA

Abstract

Real world data often exhibit inhomogeneity—complexity of the target function, noise level, etc. are not uniform over the input space. We address the issue of estimating *locally optimal kernel bandwidth* as a way to describe inhomogeneity. Estimated kernel bandwidths can be used not only for improving the regression/classification performance, but also for *Bayesian optimization* and *active learning*, i.e., we need more samples in the region where the function complexity and the noise level are higher. Our method, called *kernel mixture of kernel experts regression* (KMKER) follows the concept of *mixture of experts*, which is constituted of several complementary inference models, the so called *experts*, where in advance a latent classifier, called the *gate*, predicts the best fitting expert for each test input to infer. For the experts we implement *Gaussian process regression* models at different (global) bandwidths and a *multinomial kernel logistic regression* model as the gate.

The basic idea behind mixture of experts is, that several distinct ground truth functions over a joint input space drive the observations, which one may want to disentangle. Each expert is meant to model one of the incompatible functions such that each expert needs its individual set of hyperparameters. We differ from that idea in the sense that we assume only one ground truth function which however exhibits spacially inhomogeneous behavior. Under these assumptions we share the hyperparameters among the experts keeping their number constant.

We compare KMKER to previous methods (which cope with inhomogeneity but do not provide the optimal bandwidth estimator) on artificial and benchmark data and analyze its performance and capability for interpretation on datasets from quantum chemistry. We also demonstrate how KMKER can be applied for automatic adaptive grid selection in fluid dynamics simulations.

1. Introduction

Coping with inhomogeneity is an important issue to make machine learning techniques adjust to real data. Fig. 1 (left) shows a motivating toy example of a noisy down-chirp signal, where intuitively the *true* function complexity shrinks with growing input. Other inhomogeneities are heteroscedastic structure of noise and skewness in the distribution of training inputs.

*. K.-R. Müller is also with the Department of Brain and Cognitive Engineering, Korea University, Anam-dong, Seongbuk-gu, Seoul 02841, Korea

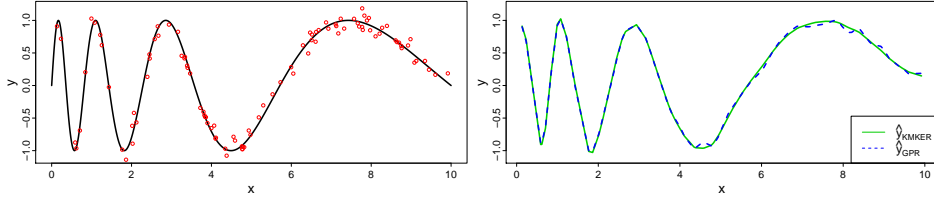


Figure 1: The oscillating function dataset (left), and the label predictions (right), with the proposed method KMKER (green) compared to standard GPR (blue). Predictions are based on 100 training examples. See Section 5.1 for a detailed specification.

Our focus in this paper is to identify these inhomogeneities jointly in terms of *locally optimal kernel bandwidth*, assuming that we use a scalable *radial basis function* (RBF)-kernel such as the Gaussian kernel

$$k^\Sigma(x, y) = \exp \left\{ -\frac{1}{2} \|\Sigma^{-1}(x - y)\|_2^2 \right\},$$

which resolution can be controlled by the positive definite bandwidth matrix Σ .

When comparing a global, isotropic bandwidth *Gaussian process regression* (GPR) model to a locally adaptive bandwidth model like the proposed KMKER model, we can see in Fig. 1 (right), that the global GPR model is not able to deal with the high and low frequencies of the data simultaneously: The optimal GPR bandwidth models the high frequency region adequately while overmodulating in the low frequency region. In contrast, KMKER models the problem with increasing bandwidth from the left to the right, as depicted by the green curve in Fig. 2—therefore reproducing the true function more accurately in Fig. 1 (right).

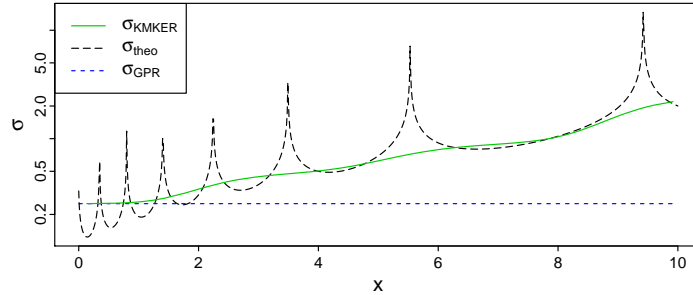


Figure 2: Bandwidths for the oscillating function dataset.

As we will show in Section 5, knowing the inhomogeneity highly improves the regression/classification performance. It is also useful for *active learning* and *Bayesian optimization*, where we need more samples in the region where the function complexity and the noise levels are higher for efficient *exploration*.

More formally, consider a regression problem, where we estimate a function f from noisy observations $y_i = f(x_i) + \varepsilon_i, i \in \{1, \dots, n\}$ where the ε_i are independent, with mean $\mathbb{E}[\varepsilon_i] = 0$ and local noise variance $\mathbb{V}[\varepsilon_i] = v(x_i)$.

In the one-dimensional case, the relation between the optimal bandwidth (for a *local linear smoother*, see Appendix A) and the inhomogeneity including the complexity of the function, noise level, and the distribution of the training data has been theoretically analyzed:

Proposition 1 (*Fan and Gijbels, 1992*) *For sample size n large enough, the optimal bandwidth to a linear least squares fit localized in x can asymptotically be decomposed as*

$$\sigma_{theo}(x) = c_n \left[\frac{v(x)}{f''(x)^2 p(x)} \right]^{\frac{1}{5}} \quad (1)$$

where p is the sample density, f'' is the second derivative of f and c_n is a constant with respect to x decreasing in n .

Note that this decomposition does not hold where f'' vanishes, as can be seen by the poles of the black curve in Fig. 2. However, intuitively an optimal bandwidth will still exist.

In the general, d -dimensional case, when additionally restricting to isotropic solutions, there also exists a decomposition $\Sigma_{theo}(x)$ that depends on the *Hessian* H_f of f . But even if the decomposition was unrestrictively valid, estimating its components has too much degrees of freedom to be considered stable. Our approach is to model $\Sigma_{opt}(x)$ directly while trying to keep the model complexity low. First of all we restrict ourselves to optimal bandwidth matrices of the form $\Sigma_{opt}(x) = \sigma_{opt}(x)\Sigma$, where $\sigma_{opt}(x)$ is scalar-valued and Σ is a diagonal matrix. Σ models the global importance of individual features, whereas $\sigma_{opt}(x)$ accounts for the spacial inhomogeneities. We adapt existing approaches from *automatic relevance determination* (ARD) to model Σ and *heteroscedastic kernel ridge regression* (Cawley et al., 2006) to model $v(x)$, whenever applicable to the data. However, there exist limited approaches to model $\sigma_{opt}(x)$, especially when it comes to go beyond trivial 1-dim toy-examples. Existing approaches tremendously suffer from the vast degrees of freedom for modelling σ_{opt} in higher dimensional real-world scenarios.

As a preliminary consideration let $\mathcal{E}: \mathcal{X} \times \mathbb{R}^+ \rightarrow \mathbb{R}, (x, \sigma) \mapsto E(x, \sigma)$ be a performance measure for predicting the label of x using bandwidth σ . \mathcal{E} could be a squared error or a negative log-likelihood estimate. Then we would like to find

$$\hat{\sigma}_{opt} = \underset{\sigma \in \mathcal{C}^0(\mathcal{X}, \mathbb{R}^+)}{\operatorname{argmin}} \int_{\mathcal{X}} \mathcal{E}(x, \sigma(x)) p(x) dx.$$

For example we could try to fit a kernel model $\log(\sigma)(x) = \sum_{i=1}^n \beta_i k(x_i, x)$, minimizing

$$\hat{\beta} = \underset{\beta}{\operatorname{argmin}} \sum_{i=1}^n \mathcal{E}(x_i, \sigma(x_i)) + \gamma \beta^\top K \beta.$$

Unfortunately, estimating $\mathcal{E}(x_i, \sigma(x_i))$ for a general $\sigma(x_i)$ -input is computationally infeasible. For example, if $\mathcal{E}(x_i, \sigma(x_i))$ is the leave-one-out GPR squared residual, then we would have to solve n GPR models after each update of β , giving a $\mathcal{O}(n^4)$ -method in computation time.

We could avoid that by also fitting $\hat{\mathcal{E}}$ from the augmented dataset $\left(\begin{pmatrix} x_i \\ \sigma_j \end{pmatrix}, \mathcal{E}(x_i, \sigma_j) \right)_{ij}$ for a finite bandwidth grid $0 < \sigma_1 < \dots < \sigma_L$. However, the augmented dataset is quite large and when it comes to adaption of hyperparameters, $\hat{\mathcal{E}}$ must be refitted over and over again.

Consider the more general objective

$$\hat{\mu} = \underset{\mu \in \mathcal{C}^0(\mathcal{X}, \mathcal{P}(\mathbb{R}^+))}{\operatorname{argmin}} \int_{\mathcal{X} \times \mathbb{R}^+} \mathcal{E}(x, \sigma) \mu_x(\sigma) p(x) d\sigma dx,$$

where we assume $x \mapsto \mu_x$ to be a continuous mapping and $\mu_x \in \mathcal{P}(\mathbb{R}^+)$ is a probability measure for $\sigma_{\text{Opt}}(x)$, that is, $\mu_x(S) = \mathbb{P}(\sigma_{\text{Opt}}(x) \in S)$ for $S \subset \mathbb{R}^+$.

This objective is a generalization of the previous one, considering the dirac measures $\mu_x(\{\sigma(x)\}) = 1$. While this objective is more powerful it is even harder to fit in its general form. However, if we restrict $\mu \in \mathcal{C}^0(\mathcal{X}, \mathcal{P}(\mathbf{S}))$ for the finite set $\mathbf{S} = \{0 < \sigma_1 < \dots < \sigma_L\}$, then the objective simplifies to a latent bandwidth classification problem, fitting the ME framework. This classifier—also called *gate*—is given by:

$$Q(x)_i \leftarrow \mathbb{P}(\sigma_{\text{Opt}}(x) = \sigma_j).$$

We will implement a soft classifier via *multinomial kernel logistic regression* MKLR. For example, we set up $\sigma_j = \sigma_{\text{GPR}} \cdot 10^{\frac{j-2}{3}}$, $1 \leq j \leq 6$ for the oscillating data. The resulting gate responses can be seen in Fig. 3.

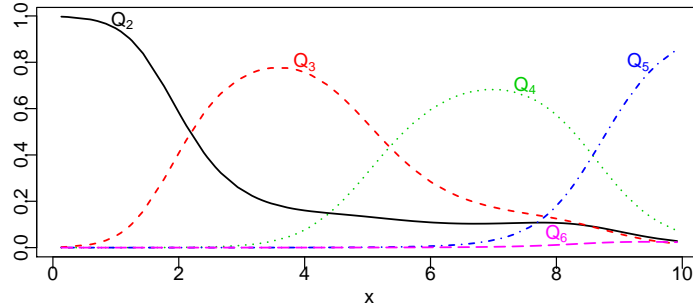


Figure 3: Gate responses for the relevant bandwidths of the oscillating data example.

While this plot is moderately comprehensible in the 1-dim case, it becomes confusing in higher dimensions. For the sake of visualization we therefore define the summary

$$\sigma_{\text{KMKER}}(x) = \exp \mathbb{E} [\log(\sigma_{\text{Opt}})|x] = \exp \left(\sum_{j=1}^L Q(x)_j \log(\sigma_j) \right) \quad (2)$$

The green curve in Fig. 2 shows an example for σ_{KMKER} for the oscillating data.

Note that σ_{KMKER} is however not in general a proper estimate for σ_{Opt} . For example consider the situation where we face a region in input space with high complexity, but scarce training data. Then it may be equally likely to deduce either high complexity with low noise, or low complexity with high noise, such that the extremes $Q(x)_1$ and $Q(x)_L$ are most likely. But the estimate $\sigma_{\text{KMKER}}(x)$ is (logarithmically) half way between them, not reflecting the situation correctly.

We will organize the paper as follows: To start with, we will discuss related work, some of which addresses local bandwidth estimation only indirectly. In Sec. 3 we will introduce mathematical notation and prepare some basic machine learning concepts. This is done in such a way so that we can reuse them modularly in our proposed method in Sec. 4. We

will then demonstrate the capabilities of our novel approach not only to improve prediction performance, but also to give interpretable insights in applications of quantum-chemistry and to guide adaptive grid selection in numerical simulations. Finally, we conclude in Sec. 6.

2. Related work

Several methods were proposed for better prediction performance in inhomogeneous data. In its basic form *Multiple kernel learning* (MKL) prepares complementary kernels $\{k^1, \dots, k^L\}$, e.g., an RBF-kernel at different scales, and use the mixed kernel $k_\mu = \sum_{j=1}^L \mu_j k^j$, where the mixing weight vector μ along with the dual variables α is optimized in a single framework. Although MKL copes with inhomogeneity to some extent, this approach uses a single mixed kernel globally over the input space and is therefore too restrictive. There exist more sophisticated versions of MKL (see Gönen and Alpaydm (2011) for a summary). For example (Gönen and Alpaydm, 2010) proposed a localized MKL approach—where a local weighting $\mu(x)$ (in the above sense of MKL) is learnt. We tried to adopt this approach, letting the kernel functions k^j be RBF-kernels at different bandwidths. Unfortunately, the objective of this approach suffers from local optima making it impractical in real-world applications.

Learning such a local weighting makes localized MKL an instance of *mixture of experts* (ME)—the concept that we also pursue in this paper. Yuksel et al. (2012) give an introduction and summary of ME approaches. A fundamental assumption of the ME model is that the overall problem to infer is too complex for a single, comparably simple expert. This is the case, for example in regression of nonstationary or piecewise continuous data, and naturally in classification where each cluster shape may follow its own pattern. In such a scenario each expert of the ME model can specialize on modelling an individual, incompatible¹ subset of the data, where the gate learns a soft assignment of data to the experts.

Under these assumptions it suggests itself to tune the hyperparameters of each expert individually on the respective assigned data subset. In the light of this paradigm there exist several instances of mixture of Gaussian processes, for example (Tresp, 2001; Meeds and Osindero, 2006; Yuan and Neubauer, 2009; Yang and Ma, 2011; Chen et al., 2014).

In this paper we break with this paradigm in the sense that we assume that each single expert is capable of modelling the whole problem, given enough training data. That is, we drop the incompatibility assumption. Yet we assume that—locally dependent—some experts perform superior compared to the others. While we still try to soft-partition the data with respect to the well performing experts, we let all experts share one set of hyperparameters, since they all model the same function.

There have been attempts to learn the model

$$\hat{f}(x) = \sum_{i=1}^n \sum_{j=1}^L \alpha_i^j k^j(x_i, x) \quad (3)$$

for individual coefficient vectors α^j corresponding to a single kernel k^j , where k^j may for example be a Gaussian kernel with bandwidth σ_j . *Multi-scale support vector regression* (MS-SVR) (Zheng et al., 2006) minimizes a loss function similar to SVR with stacked constraints for each candidate bandwidth. *Hierarchical SVR* (HSVR) (Ferrari et al., 2010) is

1. through the lens of a single expert

another approach, where several single-scale SVR models are trained, beginning with a coarse bandwidth, followed by successively fitting the current residuals with a finer bandwidth.

Both approaches provide no access to a local bandwidth estimator. This is mainly because neither the amplitude of coefficients α_i^j nor the positions of support vectors with respect to a bandwidth σ_j do necessarily match the region in the input space where this bandwidth is locally optimal.

In kernel basis pursuit (KBP) (Guigue et al., 2005), features $k^j(x_i, \cdot)$ are selected iteratively updating the prediction. In an iteration one selects the feature that is most correlated with the current residuals. KBP was however shown to be inferior to (MS-SVR).

There exist tentative approaches, e.g. Ye et al. (2006), to model σ_{opt} from Proposition 1 by estimating all components v, H_f and p separately. Combining several estimates however suffers from error exponentiation. Such an approach is especially likely to fail for high dimensional, real world data due to the growing complexity of modelling H_f .

One may also tune the bandwidths and/or centers of the radial basis functions individually, as done in *sparse multi-scale Gaussian process regression* (Walder et al., 2008) and in the adaptive spherical Gaussian kernel *relevance vector machine* approach by (Yuan et al., 2009).

Note that there are approaches to deal with heteroscedasticity, assuming that f is homogeneously complex (Kersting et al., 2007; Cawley et al., 2006). However we would like to emphasize that heteroscedasticity is an inhomogeneity which is complementary—though not independent—to optimal bandwidth.

To the best of our knowledge, no method to estimate the optimal bandwidth function in the general case in a practical manner has been proposed.

3. Preliminaries

In this section, we introduce some techniques and notation, on which our proposed method is based. To start with, we define some mathematical notation: Let $A, C \in \mathbb{R}^{m_1 \times n_1}$, $B \in \mathbb{R}^{m_2 \times n_2}$.

- $A \otimes B = \begin{bmatrix} B_{11}A & \cdots & B_{1n_2}A \\ \vdots & & \vdots \\ B_{m_21}A & \cdots & B_{m_2n_2}A \end{bmatrix}$ is the Kronecker product
- $A \odot C = [A_{ij}C_{ij}]_{ij}$ is the Hadamard, or pointwise product
- In analogy we define by $A \oslash C = [A_{ij}/C_{ij}]_{ij}$ the pointwise division
- $\mathbf{diag}(v) = \begin{bmatrix} v_1 & 0 & \cdots & 0 \\ 0 & \ddots & \ddots & \vdots \\ \vdots & \ddots & \ddots & 0 \\ 0 & \cdots & 0 & v_n \end{bmatrix}$ is the matrix with the entries of $v \in \mathbb{R}^n$ on its diagonal
- $\mathbf{1}_n = [1 \quad \cdots \quad 1]^\top \in \mathbb{R}^n$ the length-n vector of ones
- $\mathcal{I}_n = \mathbf{diag}(\mathbf{1}_n)$ the identity matrix in $\mathbb{R}^{n \times n}$

3.1 Mixture of Experts

In the ME paradigm we assume an observation to be generated by one of several processes with distinct behavior. The probability that a specific process drives the observation varies over the input space. If the supports of the processes, that is, where the respective generating probability is not negligible, overlap at most moderately, then we can cluster the input space with respect to the generating processes. In that sense, assigning the most probable generating process to an input can be formulated as a hidden classification problem.

Let (\mathbf{X}, \mathbf{Y}) be the training set of size n and let \mathbf{Z} be hidden multinomial variables

$$\mathbf{Z}_{ij} = \begin{cases} 1, & \text{process } j \text{ generated } y_i \\ 0, & \text{else} \end{cases}.$$

indicating the generating one of L potential processes. Finally, let $\Theta = \{\theta_g, \theta_{e_1}, \dots, \theta_{e_L}\}$ be the set of all model parameters for describing both, the expert models $\mathbb{P}(\mathbf{Y}|\mathbf{X}, \theta_{e_j})$ when assuming process j to drive the observations, and the probability $\mathbb{P}(\mathbf{Z}|\mathbf{X}, \theta_g)$ that specific processes drive the observations. Then we can write the observation likelihood as

$$\mathbb{P}(\mathbf{Y}|\mathbf{X}, \Theta) = \sum_{\mathbf{Z}} \mathbb{P}(\mathbf{Y}|\mathbf{X}, \mathbf{Z}, \theta_{e_1}, \dots, \theta_{e_L}) \mathbb{P}(\mathbf{Z}|\mathbf{X}, \theta_g).$$

With respect to maximizing the observation likelihood, the optimal Θ can be estimated iteratively via *expectation maximization* (EM):

In the E-step, we estimate the posterior distribution of the hidden variable $\mathbf{Z}^{(t)} \sim \mathbb{P}(\mathbf{Z}|\mathbf{X}, \mathbf{Y}, \Theta^{(t)})$ given the current set of parameters $\Theta^{(t)}$. In the M-step, we update the parameters such that the augmented log-likelihood is maximized

$$\Theta^{(t+1)} \leftarrow \underset{\Theta}{\operatorname{argmax}} \mathbb{E}_{\mathbf{Z}^{(t)}} \log \mathbb{P}(\mathbf{Y}, \mathbf{Z}^{(t)}|\mathbf{X}, \Theta).$$

If the observations \mathbf{Y} are mutually independent, conditionally on \mathbf{X} , then the EM-procedure can be simplified: In the E-step, we can factorize the hidden variable posterior

$$\mathbf{P}_{ij}^{(t)} = \mathbb{P}(\mathbf{Z}_{ij} = 1|\mathbf{X}, \mathbf{Y}, \Theta^{(t)}) = \frac{\mathbb{P}(\mathbf{Z}_{ij} = 1|x_i, \theta_g^{(t)}) \mathbb{P}(y_i|x_i, \theta_{e_j}^{(t)})}{\sum_{k=1}^L \mathbb{P}(\mathbf{Z}_{i,k} = 1|x_i, \theta_g^{(t)}) \mathbb{P}(y_i|x_i, \theta_{e_k}^{(t)})},$$

describing the belief that process j drives the i^{th} observation, given the current set of hyperparameters $\Theta^{(t)}$.

The M-step can be reformulated as

$$\Theta^{(t+1)} \leftarrow \underset{\Theta}{\operatorname{argmax}} \underbrace{\sum_{i=1}^n \sum_{j=1}^L \mathbf{P}_{ij}^{(t)} \log \mathbb{P}(\mathbf{Z}_{ij} = 1|x_i, \theta_g)}_{R_g(\theta_g)} + \underbrace{\sum_{j=1}^L \sum_{i=1}^n \mathbf{P}_{ij}^{(t)} \log \mathbb{P}(y_i|x_i, \theta_{e_j})}_{R_{e_j}(\theta_{e_j})}.$$

This form reveals, that each expert and the gate can be optimized independently in the M-step with respect to their own set of parameters. Note that predictions of the model take the form

$$\hat{y}(x) = \mathbb{E}_z \mathbb{P}(y|x, \Theta) = \sum_{j=1}^L \mathbb{E}(y|x, \theta_{e_j}) \mathbb{P}(z_j = 1|x, \theta_g).$$

3.2 Gaussian Process Regression

As the experts we would like to choose GPR. Therefore we will introduce the standard GPR model in a way which will turn out to be convenient later on. $\hat{y}_{\text{GPR}}^{\sigma_1} \mathcal{GP}(m, \lambda, \sigma_\varepsilon^2, \sigma_1 \Sigma)$ We assume $\mathbf{Y} \sim \mathcal{GP}(m\mathbf{1}, \mathbf{C})$ with global mean m and covariance function

$$\mathbf{C}(\mathbf{X}) = \sigma_\varepsilon^2(\exp(\lambda_f)\mathbf{K}^\Sigma(\mathbf{X}) + \mathcal{I}_n),$$

where

$$\Sigma = \text{diag}(\exp(\sigma_1^x), \dots, \exp(\sigma_d^x))$$

and kernel matrix $\mathbf{K}^\Sigma(\mathbf{X}) = [k^\Sigma(x_i, x_j)]_{i,j=1}^n$ and Gaussian kernel function

$$k^\Sigma(x_i, x_j) = \exp\left\{-\frac{1}{2}(x_i - x_j)^\top \Sigma^{-2}(x_i - x_j)\right\}.$$

For a test instance (x^*, y^*) , the predictive likelihood is given by

$$\mathbb{P}(y^* | x^*, \mathbf{X}, \mathbf{Y}) \sim \mathcal{N}[\mu^*(x^*), \sigma^*(x^*)],$$

where

$$\mu^*(x^*) = m + c^* \overline{\mathbf{C}}(\mathbf{Y} - m\mathbf{1}), \quad (4)$$

$$\sigma^*(x^*) = c^{**} - c^* \overline{\mathbf{C}}(c^*)^\top, \quad (5)$$

and we denote $\overline{\mathbf{C}} = \mathbf{C}^{-1}$ and

$$\mathbf{C}(\mathbf{X} \cup \{x^*\}) = \begin{bmatrix} \mathbf{C} & (c^*)^\top \\ c^* & c^{**} \end{bmatrix}.$$

Test predictions are given by

$$\hat{y}^* = \mathbb{E}[y^* | x^*, \mathbf{X}, \mathbf{Y}] = \mu^*(x^*). \quad (6)$$

For later use, we formulate the GPR predictions in Algorithm 1.

Algorithm 1 $\hat{\mathbf{Y}}^* \leftarrow \text{predict}_{\text{GPR}}(\mathbf{X}^* | \mathbf{X}, \mathbf{Y}, m, \lambda_f, \sigma_\varepsilon, \Sigma)$

Input

-
- 1: Training data $\mathbf{X} = [x_1, \dots, x_n]^\top \in \mathbb{R}^{n \times d}$, $\mathbf{Y} = [y_1, \dots, y_n]^\top \in \mathbb{R}^n$
 - 2: GPR hyper-parameters $m, \lambda_f, \sigma_\varepsilon, \Sigma$
 - 3: Test input data $\mathbf{X}^* = [x_1^*, \dots, x_T^*]^\top \in \mathbb{R}^{T \times d}$
-

Output

-
- 4: Predictions $\hat{\mathbf{Y}}^* \in \mathbb{R}^T$
-

Procedure

-
- 5: Estimate $\mathbf{C} = \sigma_\varepsilon^2(\exp(\lambda_f)\mathbf{K}^\Sigma(\mathbf{X}) + \mathcal{I}_n)$
 - 6: Solve $\mathbf{C}\alpha = \mathbf{Y} - m\mathbf{1}_n$ for α
 - 7: Predict $\hat{y}^* \leftarrow m\mathbf{1}_T + \sigma_\varepsilon^2 \exp(\lambda_f)\mathbf{K}^\Sigma(\mathbf{X}^*, \mathbf{X})\alpha$
-

Let $\theta_e = (m, \lambda_f, \sigma_\varepsilon, \sigma_1^x, \dots, \sigma_d^x)$ be the set of the GPR hyperparameters. Typically one tunes θ_e by minimizing the observation negative log-likelihood

$$-\log \mathbb{P}(\mathbf{Y}|\mathbf{X}, \theta_e) \propto \frac{1}{2} \log |\det(\mathbf{C})| + \frac{1}{2} (\mathbf{Y} - m\mathbb{1})^\top \overline{\mathbf{C}} (\mathbf{Y} - m\mathbb{1}).$$

However, for reasons that become clear later, we will minimize the weighted leave-one-out negative log predictive likelihood instead:

$$\ell_e(\mathbf{X}, \mathbf{Y}, \theta_e, P) = - \sum_{i=1}^n P_i \log \mathbb{P}(y_i|x_i, \mathbf{X}_{-i}, \mathbf{Y}_{-i}) \propto \sum_{i=1}^n \frac{P_i}{2} \left[\frac{R_i^2}{\sigma_\varepsilon^2 V_i} + \log(V_i) + \log(\sigma_\varepsilon^2) \right], \quad (7)$$

where we rewrite the leave-one-out predictive variances as $\sigma_\varepsilon^2 V$ with

$$V_i = (\overline{\mathbf{D}}_{ii})^{-1}$$

and the leave-one-out residuals as

$$looR = looY - m \cdot loo\mathbb{1}$$

with

$$looY = \mathbf{diag}(V) \overline{\mathbf{D}} \mathbf{Y}, \quad loo\mathbb{1} = \mathbf{diag}(V) \overline{\mathbf{D}} \mathbb{1}$$

for $\overline{\mathbf{D}} = \sigma_\varepsilon^2 \overline{\mathbf{C}}$. Then

$$\frac{d\ell_e(\mathbf{X}, \mathbf{Y}, \theta_e, P)}{d\sigma_\varepsilon^2} = 0 \Leftrightarrow \sigma_\varepsilon^2 \leftarrow \frac{1}{\mathbb{1}^\top P} looR^\top \mathbf{diag}(P) \mathbf{diag}(V)^{-1} looR$$

Therefore the optimal noise variance estimate relates to the weighted mean squared residual, which is intuitive. Furthermore

$$\frac{d\ell_e(\mathbf{X}, \mathbf{Y}, \theta_e, P)}{dm} = 0 \Leftrightarrow m \leftarrow \frac{loo\mathbb{1}^\top \mathbf{diag}(P) \mathbf{diag}(V)^{-1} looY}{loo\mathbb{1}^\top \mathbf{diag}(P) \mathbf{diag}(V)^{-1} loo\mathbb{1}}.$$

Therefore the optimal mean estimate relates to the weighted mean output. The remaining parameters are contained in $\overline{\mathbf{D}}$. Define

$$A_p = -\frac{d\overline{\mathbf{D}}}{dp} = \overline{\mathbf{D}} \frac{d\mathbf{D}}{dp} \overline{\mathbf{D}}.$$

Then

$$\frac{d\ell_e(\mathbf{X}, \mathbf{Y}, \theta_e, P)}{dp} = \frac{1}{2\sigma_\varepsilon^2} \mathbb{1}^\top [P \odot \mathbf{diag}(A_p) \odot [\sigma_\varepsilon^2 V + looR \odot looR]] - \frac{1}{\sigma_\varepsilon^2} (looR \odot P)^\top A_p (\mathbf{Y} - m\mathbb{1}).$$

It is $A_{\lambda_f} = \overline{\mathbf{D}}(I - \overline{\mathbf{D}})$ and $A_{\sigma_k^x} = \exp(-2\sigma_k^x) [d^k(\mathbf{X}) \odot (\mathbf{D} - I)]$, where

$$d^k(\mathbf{X})_{ij} = (x_i^k - x_j^k)^2$$

is the coordinate-wise squared distance matrix.

With this we perform gradient descent for λ_f and $\sigma_1^x, \dots, \sigma_d^x$ until convergence, applying the closed-form updates for m and σ_ε^2 in each iteration.

3.3 Multinomial Kernel Logistic Regression

We will introduce MKLR since we implement it as the gate for our ME model. Let \mathbf{X} be the training data with class membership probabilities $[\mathbf{P}, P_L]$, where $\mathbf{P} = [P_1, \dots, P_{L-1}] \in [0, 1]^{n \times (L-1)}$ with $P_L = \mathbb{1}_n - \mathbf{P}^\top \mathbb{1}_{L-1} \in [0, 1]^n$. Note that this is a generalization of the common case where we have class labels rather than probabilities such that $\mathbf{P} \in \{0, 1\}^{n \times (L-1)}$. Let $\theta_g = (\Sigma_g, \lambda_g)$ be the bandwidth and regularization parameter of the MKLR model. MKLR estimates class membership probabilities via

$$Q(x)_j = \mathbb{P}(z_j = 1 | x, \omega, \theta_g) = \frac{q(x)_j}{1 + \sum_{k=1}^{L-1} q(x)_k},$$

where

$$\omega = \begin{bmatrix} \boldsymbol{\alpha} \\ \mathbf{b} \end{bmatrix} = \begin{bmatrix} \alpha_1 & \cdots & \alpha_{L-1} \\ b_1 & \cdots & b_{L-1} \end{bmatrix}$$

are the feature weights and biases and where $q(x)_j = \exp(\mathbf{K}^{\Sigma_g}(x, \mathbf{X})\alpha_j + b_j)$ for $j < L$ and $q(x)_L = 1$ to avoid over-parameterization. Define $\mathbf{Q} = [Q_1, \dots, Q_{L-1}]$ with $Q_j = [q(x_i)_j]_{i=1}^n$. The optimal ω is defined as the minimizer of the regularized negentropy

$$\ell_g(\omega, \mathbf{X}, \mathbf{P}, \theta_g) = - \sum_{i=1}^n \sum_{j=1}^{L-1} \mathbf{P}_{ij} \log(\mathbf{Q}_{ij}) + \sum_{i=1}^n \log \left(1 + \sum_{j=1}^{L-1} \mathbf{Q}_{ij} \right) + \lambda_g \sum_{j=1}^{L-1} \alpha_j^\top \mathbf{K}^{\Sigma_g}(\mathbf{X}) \alpha_j$$

For later use, we formulate the MKLR predictions in Algorithm 2.

Let \mathbf{vec} be the vectorization of a matrix obtained by concatenation of its columns. Then

$$\nabla_g(\omega) = \frac{d\ell_g(\omega, \mathbf{X}, \mathbf{P}, \theta_g)^\top}{d\mathbf{vec}(\omega)} = (\mathcal{I}_{L-1} \otimes \widetilde{\mathbf{K}}) \mathbf{vec}(\mathbf{S}),$$

where

$$\widetilde{\mathbf{K}} = \begin{bmatrix} \mathbf{K} & 0 \\ \mathbb{1}^\top & -\lambda_g \end{bmatrix}$$

and $\mathbf{S} = [S_1, \dots, S_{L-1}]$ with $S_j = \begin{bmatrix} Q_j - P_j + \lambda_g \alpha_j \\ \mathbb{1}^\top \alpha_j \end{bmatrix}$.

Note that there is no closed form solution for $\nabla_g(\omega) = 0$. Fortunately, the objective is convex such that we can approximate the solution via *iteratively reweighted least squares*, performing *Newton-Raphson* updates on the gradient to find its unique root via

$$\mathbf{vec}(\omega) \leftarrow \mathbf{vec}(\omega) - \mathbf{H}_g(\omega)^{-1} \nabla_g(\omega),$$

where the Hessian is given by

$$\begin{aligned} \mathbf{H}_g(\omega) &= \frac{d^2 \ell_g(\omega, \mathbf{X}, \mathbf{P}, \theta_g)}{d^2 \mathbf{vec}(\omega)} = \mathcal{I}_{L-1} \otimes \begin{bmatrix} \lambda_g \mathbf{K} & 0 \\ 0 & 0 \end{bmatrix} \\ &+ \mathcal{I}_{L-1} \otimes \begin{bmatrix} \mathbf{K} \\ \mathbb{1}^\top \end{bmatrix} \left[\mathbf{diag}(\mathbf{vec}(\mathbf{Q})) - \begin{bmatrix} \mathbf{diag}(Q_1) \\ \vdots \\ \mathbf{diag}(Q_{L-1}) \end{bmatrix} [\mathbf{diag}(Q_1), \dots, \mathbf{diag}(Q_{L-1})] \right] \mathcal{I}_{L-1} \otimes [\mathbf{K}, \mathbb{1}], \end{aligned}$$

Algorithm 2 $\mathbf{Q}^* \leftarrow \text{predict}_{\text{MKLR}}(\mathbf{X}^* | \mathbf{X}, \mathbf{P}, \Sigma_g, \lambda_g)$

Input

- 1: Training inputs $\mathbf{X} = [x_1, \dots, x_n]^\top \in \mathbb{R}^{n \times d}$ and training labels/probabilities $\mathbf{P} = [P_1, \dots, P_{L-1}]^\top \in [0, 1]^{n \times (L-1)}$
 - 2: MKLR hyper-parameters Σ_g, λ_g
 - 3: Test input data $\mathbf{X}^* = [x_1^*, \dots, x_T^*]^\top \in \mathbb{R}^{T \times d}$
-

Output

- 4: Test class assignments $\mathbf{Q}^* \in [0, 1]^{T \times L}$
-

Procedure

- 5: Initialize $\boldsymbol{\alpha} = 0$, $\mathbf{b} = \frac{1}{n} \mathbb{1}_n^\top \mathbf{P}$
 - 6: Estimate $B = \frac{1}{2} (\mathcal{I}_{L-1} - \frac{1}{L} \mathbb{1}_{L-1} \mathbb{1}_{L-1}^\top)$ with eigen decomposition $B = V \text{diag}(D) V^\top$
 - 7: Estimate kernel matrix $\mathbf{K}^{\Sigma_g}(\mathbf{X})$ with eigen decomposition $\mathbf{K}^{\Sigma_g}(\mathbf{X}) = U_g \text{diag}(\Lambda_g) U_g^\top$
 - 8: Virtually define $\widetilde{\mathbf{M}}^{-1} = (V \otimes U_g) [\text{diag}(D \otimes \Lambda_g) + \lambda_g \mathcal{I}_{n(L-1)}]^{-1} (V^\top \otimes U_g^\top) \triangleright$ Don't calculate explicitly!
 - 9: Estimate $\mathbf{N}^{-1} = (\mathcal{I}_{L-1} \otimes \mathbb{1}_n^\top) \widetilde{\mathbf{M}}^{-1} (B \otimes \mathbb{1}_n)$ and solve for \mathbf{N} \triangleright according to (8)
 - 10: **while** $\boldsymbol{\alpha}$ not converged **do**
 - 11: Set $\mathbf{Q} = \exp(\mathbf{K}^{\Sigma_g}(\mathbf{X}) \boldsymbol{\alpha} + \mathbb{1}_n \mathbf{b})$
 - 12: Normalize $\mathbf{Q} = \text{diag}(\mathbb{1}_n + \mathbf{Q} \mathbb{1}_{L-1})^{-1} \mathbf{Q}$
 - 13: Set $\mathbf{R} = \mathbf{Q} - \mathbf{P} + \lambda_g \boldsymbol{\alpha}$
 - 14: $\text{vec}(\Delta \mathbf{b}) = \mathbf{N} \left((\mathcal{I}_{L-1} \otimes \mathbb{1}^\top) \widetilde{\mathbf{M}}^{-1} \text{vec}(\mathbf{R}) - \boldsymbol{\alpha}^\top \mathbb{1} \right)$ \triangleright according to (9)
 - 15: $\text{vec}(\Delta \boldsymbol{\alpha}) = \widetilde{\mathbf{M}}^{-1} \text{vec}(\mathbf{R} - (\Delta \mathbf{b} B) \otimes \mathbb{1}_n)$ \triangleright according to (10)
 - 16: Update $\boldsymbol{\alpha} = \boldsymbol{\alpha} - \Delta \boldsymbol{\alpha}$, $\mathbf{b} = \mathbf{b} - \Delta \mathbf{b}$
 - 17: Set $\mathbf{Q}^* = [\exp(\mathbf{K}^{\Sigma_g}(\mathbf{X}^*, \mathbf{X}) \boldsymbol{\alpha} + \mathbb{1}_T \mathbf{b}), \mathbb{1}_T]$
 - 18: Normalize $\mathbf{Q}^* \leftarrow \text{diag}(\mathbf{Q}^* \mathbb{1}_L)^{-1} \mathbf{Q}^*$
-

Solving $\mathbf{H}_g(\omega)^{-1} \nabla_g(\omega)$ in each iteration is however a computational bottleneck. In the multi-class case, solving one such system of $n(L-1)$ linear equations may already be infeasible. To circumvent both problems, we instead use the bound optimization technique according to [Böhning, 1992], where the Hessian is replaced by an upper bound positive definite matrix $\mathbf{B} \geq \mathbf{H}_g(\omega)$ in the sense of *Loewner ordering*, that is, $\mathbf{B} - \mathbf{H}_g(\omega)$ is positive semi-definite. Such an upper bound is given by

$$\mathbf{B} = B \otimes \begin{bmatrix} \mathbf{K} \\ \mathbb{1}^\top \end{bmatrix} [\mathbf{K}, \mathbb{1}] + \mathcal{I}_{L-1} \otimes \begin{bmatrix} \lambda_g \mathbf{K} & 0 \\ 0 & 0 \end{bmatrix},$$

where

$$B = \frac{1}{2} \left(\mathcal{I}_{L-1} - \frac{1}{L} \mathbb{1} \mathbb{1}^\top \right).$$

Then the new update rule

$$\omega \leftarrow \omega - \Delta \omega$$

is still guaranteed to converge, where $\text{vec}(\Delta \omega) = \mathbf{B}^{-1} \nabla_g(\omega)$. We can rewrite

$$\mathbf{B} = (\mathcal{I}_{L-1} \otimes \widetilde{\mathbf{K}}) \mathbf{M},$$

with

$$\mathbf{M} = B \otimes \begin{bmatrix} \mathbf{K} & \mathbb{1} \\ 0 & 0 \end{bmatrix} + \mathcal{I}_{L-1} \otimes \begin{bmatrix} \lambda_g \mathcal{I}_n & 0 \\ \mathbb{1}^\top & 0 \end{bmatrix}.$$

Therefore we need to solve $\mathbf{M} \text{vec}(\Delta\omega) = \text{vec}(\mathbf{S})$. For this we split the system of linear equations into two groups, the rows that correspond to the update of $\boldsymbol{\alpha}$ and \mathbf{b} , respectively: Denote

$$\Delta\omega = \begin{bmatrix} \Delta\boldsymbol{\alpha} \\ \Delta\mathbf{b} \end{bmatrix}$$

and let $\widetilde{\mathbf{M}} = \mathbf{B} \otimes \mathbf{K} + \lambda_g \mathcal{I}_{n(L-1)}$ and $\mathbf{R} = \mathbf{Q} - \mathbf{P} + \lambda_g \boldsymbol{\alpha}$. Then

$$\begin{aligned} \text{vec}(\mathbf{R}) &= [\widetilde{\mathbf{M}}, \mathbf{B} \otimes \mathbb{1}] \begin{bmatrix} \text{vec}(\Delta\boldsymbol{\alpha}) \\ \text{vec}(\Delta\mathbf{b}) \end{bmatrix} = \widetilde{\mathbf{M}} \text{vec}(\Delta\boldsymbol{\alpha}) + (\mathbf{B} \otimes \mathbb{1}) \text{vec}(\Delta\mathbf{b}) \\ \Leftrightarrow \text{vec}(\Delta\boldsymbol{\alpha}) &= \widetilde{\mathbf{M}}^{-1} \text{vec}(\mathbf{R} - (\Delta\mathbf{b}\mathbf{B}) \otimes \mathbb{1}) \end{aligned}$$

The second set of equations are fulfilled if

$$\boldsymbol{\alpha}^\top \mathbb{1} = \mathcal{I}_{L-1} \otimes [\mathbb{1}^\top, 0] \text{vec}(\Delta\omega) = (\mathcal{I}_{L-1} \otimes \mathbb{1}^\top) \text{vec}(\Delta\boldsymbol{\alpha}).$$

Plugging in the first into the second equation we can solve for $\Delta\mathbf{b}$:

$$\begin{aligned} \boldsymbol{\alpha}^\top \mathbb{1} &= (\mathcal{I}_{L-1} \otimes \mathbb{1}^\top) \widetilde{\mathbf{M}}^{-1} \text{vec}(\mathbf{R} - (\Delta\mathbf{b}\mathbf{B}) \otimes \mathbb{1}) \\ \Leftrightarrow \text{vec}(\Delta\mathbf{b}) &= \mathbf{N} \left((\mathcal{I}_{L-1} \otimes \mathbb{1}^\top) \widetilde{\mathbf{M}}^{-1} \text{vec}(\mathbf{R}) - \boldsymbol{\alpha}^\top \mathbb{1} \right), \end{aligned}$$

where we have defined

$$\mathbf{N}^{-1} = (\mathcal{I}_{L-1} \otimes \mathbb{1}^\top) \widetilde{\mathbf{M}}^{-1} (\mathbf{B} \otimes \mathbb{1}).$$

Note that since \mathbf{N} is an $(L-1)^2$ -matrix its inversion is fast. The advantage over explicit *Newton-Raphson* updates is as follows:

First of all, since $\widetilde{\mathbf{M}}$ does not depend on ω we can calculate its inverse once and reuse it over all iterations. Moreover we can exploit the structure of $\widetilde{\mathbf{M}}$, being sum of a Kronecker product of two symmetric positive semi-definite matrices and a multiple of the identity. Therefore we can reduce the complexity of its inversion to the eigen decomposition of the two matrices $\mathbf{B} = \mathbf{V} \text{diag}(\mathbf{D}) \mathbf{V}^\top$ and $\mathbf{K}^{\Sigma_g} = \mathbf{U}_g \text{diag}(\Lambda_g) \mathbf{U}_g^\top$:

$$\widetilde{\mathbf{M}}^{-1} = (\mathbf{V} \otimes \mathbf{U}_g) [\text{diag}(\mathbf{D} \otimes \Lambda_g) + \lambda_g \mathcal{I}_{n(L-1)}]^{-1} (\mathbf{V}^\top \otimes \mathbf{U}_g^\top)$$

Finally, due to its form we neither need to calculate $\widetilde{\mathbf{M}}^{-1}$ explicitly nor we require matrix-vector multiplication in the $n(L-1)$ -dimensional space. This is because for matrices $\mathbf{A}_1 \in \mathbb{R}^{n_1 \times m_1}$, $\mathbf{A}_2 \in \mathbb{R}^{n_2 \times m_2}$, $\mathbf{A}_3 \in \mathbb{R}^{m_2 \times m_1}$ we have

$$(\mathbf{A}_1 \otimes \mathbf{A}_2) \text{vec}(\mathbf{A}_3) = \text{vec}(\mathbf{A}_2 \mathbf{A}_3 \mathbf{A}_1^\top)$$

and for $\mathbf{B}_1 \in \mathbb{R}^{m_1 \times n_3}$, $\mathbf{B}_2 \in \mathbb{R}^{m_2 \times n_4}$ we have

$$(\mathbf{A}_1 \otimes \mathbf{A}_2)(\mathbf{B}_1 \otimes \mathbf{B}_2) = (\mathbf{A}_1 \mathbf{B}_1 \otimes \mathbf{A}_2 \mathbf{B}_2).$$

For example we can calculate \mathbf{N}^{-1} efficiently via

$$\mathbf{N}^{-1} = (\mathbf{V} \otimes (\mathbb{1}_n^\top \mathbf{U}_g)) [\text{diag}(\mathbf{D} \otimes \Lambda_g) + \lambda_g \mathcal{I}_{n(L-1)}]^{-1} ((\mathbf{V}^\top \mathbf{B}) \otimes \mathbf{U}_g^\top \mathbb{1}_n). \quad (8)$$

Then the updates are given by

$$\text{vec}(\Delta \mathbf{b}) = \mathbf{N} \left(V \left[\left(U_g^\top \mathbf{R} V \right) \oslash (\Lambda_g D^\top + \lambda_g \mathbb{1}_n \mathbb{1}_{L-1}^\top) \right]^\top U_g^\top \mathbb{1}_n - \boldsymbol{\alpha}^\top \mathbb{1}_n \right) \quad (9)$$

and

$$\Delta \boldsymbol{\alpha} = U_g \left[\left(U_g^\top (\mathbf{R} - (\Delta \mathbf{b} B) \otimes \mathbb{1}) V \right) \oslash (\Lambda_g D^\top + \lambda_g \mathbb{1}_n \mathbb{1}_{L-1}^\top) \right] V^\top. \quad (10)$$

4. Proposed method

In this section, we propose our novel method KMKER.

4.1 Kernel Mixture of Kernel Experts

The classical interpretation of ME is that we observe data driven by several incompatible functions. For better inference ME tries to disentangle the training observations into disjoint subsets that follow the different generation laws. Under this assumption it is reasonable to optimize each expert model with an individual set of parameters solely based on the designated subset.

We deviate from this interpretation in the sense that we assume only one observed function, which however exhibits spacially varying complexity. With that in mind we learn each expert on the full training set regardless of the belief in affiliation to the respective component. Moreover we share a single set of hyperparameters for all experts up to an individual isotropic bandwidth scaling $\sigma_1 < \dots < \sigma_L$, i.e. $\theta_{e_j} = (m, \lambda_f, \sigma_\varepsilon, \sigma_j[\sigma_1^x, \dots, \sigma_d^x])$. Note that we hold the individual scales σ_j fixed, even though tuning would be possible. This keeps the complexity of the proposed model low which is therefore faster to tune and less prone to overfitting. Note that overfitting is a major issue for ME models.

With respect to the predictive distribution of the GPR experts the observations \mathbf{Y} are not mutually independent. This is however a necessary assumption for the training of the EM-model with the simplified EM-procedure as described in Subsection 3.1. Inspired by [?] we circumvent this problem by optimizing the leave-one-out predictive likelihood instead:

$$\prod_{i=1}^n \mathbb{P}(y_i | x_i, \mathbf{X}_{-i}, \mathbf{Y}_{-i}, \Theta) = \prod_{i=1}^n \sum_{j=1}^L \mathbb{P}(y_i | x_i, \mathbf{X}_{-i}, \mathbf{Y}_{-i}, \theta_{e_j}) \mathbb{P}(\mathbf{Z}_{ij} = 1 | x_i, \mathbf{X}_{-i}, \mathbf{Y}_{-i}, \theta_g)$$

Given our belief about the hidden variables \mathbf{Z} we can augment this likelihood via

$$\mathbb{P}(\mathbf{Y}, \mathbf{Z} | \mathbf{X}, \Theta) = \prod_{i=1}^n \prod_{j=1}^L \left[\mathbb{P}(y_i | x_i, \mathbf{X}_{-i}, \mathbf{Y}_{-i}, \theta_{e_j}) \mathbb{P}(\mathbf{Z}_{ij} = 1 | x_i, \mathbf{X}_{-i}, \mathbf{Y}_{-i}, \theta_g) \right]^{\mathbf{Z}_{ij}}.$$

From that point we can proceed similar to the standard framework of ME:

For an initial $\mathbf{P}^{(0)} \equiv \frac{1}{L}$, define the leave-one-out gate responses

$$\mathbf{Q}_{ij}^{(t)} = \mathbb{P}(\mathbf{Z}_{ij} = 1 | x_i, \mathbf{X}_{-i}, \mathbf{Y}_{-i}, \mathbf{P}_{-i}^{(t)}, \theta_g^{(t)}).$$

In the E-step we calculate

$$\mathbf{P}_{ij}^{(t)} = \mathbb{P}(\mathbf{Z}_{ij} = 1 | \mathbf{X}, \mathbf{Y}, \Theta^{(t)}) = \frac{\mathbf{Q}_{ij}^{(t-1)} \mathbb{P}(y_i | x_i, \mathbf{X}_{-i}, \mathbf{Y}_{-i}, \theta_{e_j}^{(t)})}{\sum_{k=1}^L \mathbf{Q}_{ik}^{(t-1)} \mathbb{P}(y_i | x_i, \mathbf{X}_{-i}, \mathbf{Y}_{-i}, \theta_{e_k}^{(t)})}$$

Our final objective function is given by

$$\begin{aligned} \ell^{(t)}(\mathbf{X}, \mathbf{Y}, \Theta) &= -\mathbb{E}_{\mathbf{Z}^{(t)}} \log \mathbb{P}(\mathbf{Y}, \mathbf{Z}^{(t)} | \mathbf{X}, \Theta) \\ &= \underbrace{\left[-\sum_{i=1}^n \sum_{j=1}^L \mathbf{P}_{ij}^{(t)} \log \mathbb{P}(\mathbf{Z}_{ij} = 1 | x_i, \mathbf{X}_{-i}, \mathbf{Y}_{-i}, \theta_g) \right]}_{R_g^{(t)}(\theta_g)} + \underbrace{\left[-\sum_{i=1}^n \sum_{j=1}^L \mathbf{P}_{ij}^{(t)} \log \mathbb{P}(y_i | x_i, \mathbf{X}_{-i}, \mathbf{Y}_{-i}, \theta_{e_j}) \right]}_{R_e^{(t)}(\theta_{e_1}, \dots, \theta_{e_L})} \end{aligned}$$

In the M-step we therefore minimize $\ell^{(t)}$ via

$$\Theta^{(t+1)} \leftarrow \underset{\Theta}{\operatorname{argmin}} R_g^{(t)}(\theta_g) + R_e^{(t)}(\theta_{e_1}, \dots, \theta_{e_L}),$$

where the minimizations of $R_g^{(t)}(\theta_g)$ and $R_e^{(t)}(\theta_{e_1}, \dots, \theta_{e_L})$ are independent. Note that with (7) we can rewrite

$$R_e^{(t)}(\theta_{e_1}, \dots, \theta_{e_L}) = \sum_{j=1}^L \ell_e \left(\mathbf{X}, \mathbf{Y}, \theta_{e_j}, \left[\mathbf{P}_{ij}^{(t)} \right]_i \right).$$

Due to linearity of the gradient the optimization of the shared parameters $(m, \lambda_f, \sigma_\varepsilon)$ is therefore straightforward:

As they will become handy for efficient implementation, define the matrices

$$\begin{aligned} W_j &= \mathbf{diag}(\overline{\mathbf{D}}^j), \quad loo\mathbb{1}_j = \left[\overline{\mathbf{D}}^j \mathbb{1} \right] \odot W_j, \quad looY_j = \left[\overline{\mathbf{D}}^j \mathbf{Y} \right] \odot W_j \\ A_j^\mathbb{1} &= \left(\mathcal{I} - \overline{\mathbf{D}}^j \right) \overline{\mathbf{D}}^j \mathbb{1}, \quad A_j^Y = \left(\mathcal{I} - \overline{\mathbf{D}}^j \right) \overline{\mathbf{D}}^j \mathbf{Y}, \quad d_j^A = \mathbf{diag} \left(\left(\mathcal{I} - \overline{\mathbf{D}}^j \right) \overline{\mathbf{D}}^j \right) \\ looR &= looY - m \cdot loo\mathbb{1}, \quad AR = A^Y - m \cdot A^\mathbb{1} \end{aligned}$$

Then we update

$$\begin{aligned} \frac{dR_e^{(t)}}{dm} = 0 &\Leftrightarrow m \leftarrow \frac{\mathbb{1}_n^\top [loo\mathbb{1} \odot \mathbf{P}^{(t)} \odot W \odot looY] \mathbb{1}_L}{\mathbb{1}_n^\top [loo\mathbb{1} \odot \mathbf{P}^{(t)} \odot W \odot loo\mathbb{1}] \mathbb{1}_L} \\ \frac{dR_e^{(t)}}{d\sigma_\varepsilon^2} = 0 &\Leftrightarrow \sigma_\varepsilon^2 \leftarrow \frac{1}{n} \mathbb{1}_n^\top [looR \odot \mathbf{P}^{(t)} \odot W \odot looR] \mathbb{1}_L \\ \frac{dR_e^{(t)}}{d\lambda_f} &= \frac{1}{2\sigma_\varepsilon^2} \mathbb{1}_n^\top \left[\mathbf{P}^{(t)} \odot d^A \odot [\sigma_\varepsilon^2 \odot W + looR \odot looR] - 2[looR \odot \mathbf{P}^{(t)} \odot AR] \right] \mathbb{1}_L \end{aligned}$$

Algorithm 3 train_{KMKER}

Input

- 1: Relative bandwidths $\sigma_1 < \dots < \sigma_L$ logarithmically spaced around 1
 - 2: Training data $\mathbf{X} = [x_1, \dots, x_n]^\top \in \mathbb{R}^{n \times d}$, $\mathbf{Y} = [y_1, \dots, y_n]^\top \in \mathbb{R}^n$
 - 3: Validation data $\mathbf{X}_v, \mathbf{Y}_v$
 - 4: Gate hyper-parameters $\theta_g = (\sigma_g, \lambda_g)$
-

Output

- 5: KMKER model parameters $(\mathbf{P}, m, \lambda_f, \sigma_\varepsilon, \Sigma, \sigma_g, \lambda_g, \sigma_1, \dots, \sigma_L)$
-

Procedure

- 6: Optimize $(m, \lambda_f, \sigma_\varepsilon, \sigma_1^x, \dots, \sigma_d^x)$ as described in Subsection 3.2
 - 7: Set $\Sigma = \text{diag}(\exp(\sigma_1^x), \dots, \exp(\sigma_d^x))$
 - 8: Estimate kernel matrices $\mathbf{K}^{\sigma_j \Sigma}$ for $1 \leq j \leq L$
 - 9: Estimate eigen decompositions $\mathbf{K}^{\sigma_j \Sigma} = U_j \Lambda_j U_j^\top$ for $1 \leq j \leq L$
 - 10: Initialize $\mathbf{P} = \frac{1}{L} \mathbf{1}_n \mathbf{1}_L^\top$
 - 11: **while** Err_v decreases **do**
 - 12: **for** $1 \leq i \leq n$ **do** ▷ Fit \mathbf{Q} to \mathbf{P} with Algorithm 2
 - 13: $\mathbf{Q}_i \leftarrow \text{predict}_{\text{MKLR}}(x_i | \mathbf{X}_{-i}, \mathbf{P}_{-i}, \sigma_g \Sigma, \lambda_g)$
 - 14: **for** $1 \leq j \leq L$ **do** ▷ Prepare helpful variables
 - 15: Set $\bar{\mathbf{D}}^j = U_j [\exp(\lambda_f) \Lambda_j + \mathcal{I}_n]^{-1} U_j^\top$
 - 16: $W_j = \text{diag}(\bar{\mathbf{D}}^j)$, $\text{loo}\mathbf{1}_j = \bar{\mathbf{D}}^j \mathbf{1} \otimes W_j$, $\text{loo}Y_j = \bar{\mathbf{D}}^j \mathbf{Y} \otimes W_j$
 - 17: $A_j^1 = (\mathcal{I} - \bar{\mathbf{D}}^j) \bar{\mathbf{D}}^j \mathbf{1}$, $A_j^Y = (\mathcal{I} - \bar{\mathbf{D}}^j) \bar{\mathbf{D}}^j \mathbf{Y}$, $d_j^A = \text{diag}((\mathcal{I} - \bar{\mathbf{D}}^j) \bar{\mathbf{D}}^j)$
 - 18: Set $\text{loo}R = \text{loo}Y - m \cdot \text{loo}\mathbf{1}$
 - 19: Update $\mathbf{P} \leftarrow \mathbf{Q} \odot \sqrt{W} \odot \exp(-\text{loo}R \odot \text{loo}R \odot W / (2\sigma_\varepsilon^2))$ and normalize $\mathbf{P} \leftarrow \text{diag}(\mathbf{P} \mathbf{1}_L)^{-1} \mathbf{P}$
 - 20: **while** λ_f not converged **do**
 - 21: Update $m \leftarrow \mathbf{1}_n^\top [\text{loo}\mathbf{1} \odot \mathbf{P} \odot W \odot \text{loo}Y] \mathbf{1}_L / \mathbf{1}_n^\top [\text{loo}\mathbf{1} \odot \mathbf{P} \odot W \odot \text{loo}\mathbf{1}] \mathbf{1}_L$
 - 22: Set $\text{loo}R = \text{loo}Y - m \cdot \text{loo}\mathbf{1}$, $AR = A^Y - m \cdot A^1$
 - 23: Update $\sigma_\varepsilon^2 \leftarrow \frac{1}{n} \mathbf{1}_n^\top [\text{loo}R \odot \mathbf{P} \odot W \odot \text{loo}R] \mathbf{1}_L$
 - 24: Estimate $\frac{dR_\varepsilon^{(t)}}{d\lambda_f} = \frac{1}{2\sigma_\varepsilon^2} \mathbf{1}_n^\top \left[\mathbf{P}^{(t)} \odot d^A \odot [\sigma_\varepsilon^2 \otimes W + \text{loo}R \odot \text{loo}R] - 2[\text{loo}R \odot \mathbf{P}^{(t)} \odot AR] \right] \mathbf{1}_L$
 - 25: Update $\lambda_f \leftarrow \lambda_f - \eta^{(t)} \frac{dR_\varepsilon^{(t)}}{d\lambda_f}$
 - 26: **for** $1 \leq j \leq L$ **do** ▷ Prepare helpful variables
 - 27: Set $\bar{\mathbf{D}}^j = U_j [\exp(\lambda_f) \Lambda_j + \mathcal{I}_n]^{-1} U_j^\top$
 - 28: $W_j = \text{diag}(\bar{\mathbf{D}}^j)$, $\text{loo}\mathbf{1}_j = \bar{\mathbf{D}}^j \mathbf{1} \otimes W_j$, $\text{loo}Y_j = \bar{\mathbf{D}}^j \mathbf{Y} \otimes W_j$
 - 29: $A_j^1 = (\mathcal{I} - \bar{\mathbf{D}}^j) \bar{\mathbf{D}}^j \mathbf{1}$, $A_j^Y = (\mathcal{I} - \bar{\mathbf{D}}^j) \bar{\mathbf{D}}^j \mathbf{Y}$, $d_j^A = \text{diag}((\mathcal{I} - \bar{\mathbf{D}}^j) \bar{\mathbf{D}}^j)$
 - 30: Predict validation labels according to Algorithm 4
 - 31: $\hat{\mathbf{Y}}_v \leftarrow \text{predict}_{\text{KMKER}}(\mathbf{X}_v | \mathbf{X}, \mathbf{Y}, \mathbf{P}, m, \lambda_f, \sigma_\varepsilon, \Sigma, \sigma_g, \lambda_g, \sigma_1, \dots, \sigma_L)$
 - 31: Estimate $\text{Err}_v \leftarrow \|\mathbf{Y}_v - \hat{\mathbf{Y}}_v\|^2$ ▷ Validation sum squared error
-

such that

$$\lambda_f \leftarrow \lambda_f - \eta^{(t)} \frac{dR_\varepsilon^{(t)}}{d\lambda_f}$$

We summarized the KMKER training procedure in Algorithm 3.

Predictions are done via

$$\hat{y}(x) = \mathbb{E}_z \mathbb{P}(y|x, \mathbf{X}, \mathbf{Y}, \mathbf{P}, \Theta) = \sum_{j=1}^L \mathbb{P}(z_j = 1|x, \mathbf{X}, \mathbf{Y}, \mathbf{P}, \theta_g) \mathbb{E}(y|x, \mathbf{X}, \mathbf{Y}, \theta_{e_j}) \quad (11)$$

which we summarized in Algorithm 4.

Algorithm 4 $\hat{\mathbf{Y}}^* \leftarrow \text{predict}_{\text{KMKER}}(\mathbf{X}^*|\mathbf{X}, \mathbf{Y}, \mathbf{P}, m, \lambda_f, \sigma_\varepsilon, \Sigma, \sigma_g, \lambda_g, \sigma_1, \dots, \sigma_L)$

Input

- 1: Training data $\mathbf{X} = [x_1, \dots, x_n]^\top \in \mathbb{R}^{n \times d}$, $\mathbf{Y} = [y_1, \dots, y_n]^\top \in \mathbb{R}^n$
- 2: Training bandwidths assignment probabilities $\mathbf{P} = [P_1, \dots, P_{L-1}]^\top \in [0, 1]^{n \times (L-1)}$
- 3: Shared GPR hyper-parameters $m, \lambda_f, \sigma_\varepsilon, \Sigma$
- 4: Individual GPR bandwidths $\sigma_1 < \dots < \sigma_L$
- 5: MKLR hyper-parameters σ_g, λ_g
- 6: Test input data $\mathbf{X}^* = [x_1^*, \dots, x_T^*]^\top \in \mathbb{R}^{T \times d}$

Output

- 7: Predictions $\hat{\mathbf{Y}}^* \in \mathbb{R}^T$

Procedure

- 8: Estimate test bandwidths assignment probabilities ▷ Gate predictions according to Algorithm 2
 $\mathbf{Q}^* \leftarrow \text{predict}_{\text{MKLR}}(\mathbf{X}^*|\mathbf{X}, \mathbf{P}, \sigma_g \Sigma, \lambda_g)$
 - 9: **for** $1 \leq j \leq L$ **do** ▷ Expert predictions according to Algorithm 1
 - 10: $\hat{\mathbf{Y}}^j \leftarrow \text{predict}_{\text{GPR}}(\mathbf{X}^*|\mathbf{X}, \mathbf{Y}, m, \lambda_f, \sigma_\varepsilon, \sigma_j \Sigma)$
 - 11: Predict $\hat{\mathbf{Y}}^* \leftarrow [\mathbf{Q}^* \odot [\hat{\mathbf{Y}}^1, \dots, \hat{\mathbf{Y}}^L]] \mathbf{1}_L$
-

5. Experiments

5.1 Oscillating function toy data

We begin with the toy example of a noisy down-chirp signal, as already discussed in the introduction. Let $r(x) = \sin(2\pi(0.35 \cdot 10 + 1)/(0.35x + 1))$, $x \in [0, 10]$ be the *true* function to learn. We would like to compare to the experimental setting of Zheng et al. (2006):

We generate 30 datasets $(\mathbf{X}_{(i)}, \mathbf{Y}_{(i)})$ of size 100 with inputs $x \sim \mathcal{U}\{[0, 10]\}$ and $y = r(x) + \varepsilon$, where $\varepsilon \sim \mathcal{N}(0, 0.1^2)$. An example dataset can be seen in Fig. 1 (left). The corresponding validation datasets are given by $(\mathbf{X}_{(i)}, \mathbf{r}_{(i)})$ with $\mathbf{r}_{(i)} = r(\mathbf{X}_{(i)})$. They select hyperparameters by minimizing the validation *root mean squared error* (RMSE) over the first five datasets and report performance as the average validation RMSE over all 30 datasets.

With their model, Zheng et al. (2006) report a performance of $\text{RMSE} = 0.0515$. They use four bandwidths logarithmically spaced between $\sigma_1 = 0.15$ and $\sigma_4 = 1.4$. However, they lack an analysis of a spacial bandwidth segmentation. Now that our gate $Q(x)$ is not a static hyperparameter which we can perform a grid search on, we fit the gate and the expert hyperparameters only on the first dataset minimizing its validation RMSE:

According to Algorithm 3 we perform $\text{train}_{\text{KMKER}}(\mathbf{X}_{(1)}, \mathbf{Y}_{(1)}, \mathbf{X}_{(1)}, \mathbf{r}_{(1)}, \sigma_1, \dots, \sigma_L, \sigma_g, \lambda_g)$ for several hyperparameter candidates, and found $\sigma_j = 10^{\frac{j-2}{3}}$, $1 \leq j \leq 6$, $\sigma_g = 5$, $\lambda_g = 10^{-3}$ to work well. The global GPR model within the training procedure was tuned to $\sigma_{\text{GPR}} = 0.25$. As can be seen in Fig.3, σ_2 to σ_5 are mainly used, effectively resulting in a bandwidth range from 0.25 to 2.5. The expert hyperparameters are $(m, \lambda_f, \sigma_\varepsilon) = (0.5863, 3.9631, 0.0833)$ and we are given a gate model $\mathbf{Q}_{(1)}(x) = \text{predict}_{\text{MKLR}}(x|\mathbf{X}_{(1)}, \mathbf{P}, \sigma_g \sigma_{\text{GPR}}, \lambda_g)$.

We then build the KMKER predictions similar to Algorithm 4, reusing the gate $\mathbf{Q}_{(1)}$:

$$\hat{\mathbf{r}}_{(i)} = [\mathbf{Q}_{(1)}(\mathbf{X}_{(i)}) \odot [\hat{\mathbf{Y}}_{(i)}^1, \dots, \hat{\mathbf{Y}}_{(i)}^L]] \mathbf{1}_L$$

with $\hat{\mathbf{Y}}_{(i)}^j = \text{predict}_{\text{GPR}}(\mathbf{X}_{(i)}|\mathbf{X}_{(i)}, \mathbf{Y}_{(i)}, m, \lambda_f, \sigma_\varepsilon, \sigma_j \sigma_{\text{GPR}})$. This gives a final performance of $\text{RMSE} = 0.0439 \pm 0.0024$, which is significantly better than the compared MS-SVR approach.

5.2 Boston Housing Data

The Boston housing dataset (Harrison and Rubinfeld (1978)) contains 506 regions in Boston with their median owner-occupied homes price to predict. We are given 13 features as inputs that characterize these regions, such as crime rate, nitrogen oxides concentration, property-tax rate, etc.. In the following we give a 2-dimensional visualization of the properties using *t-distributed stochastic neighbor embedding* (t-SNE) Maaten and Hinton (2008).

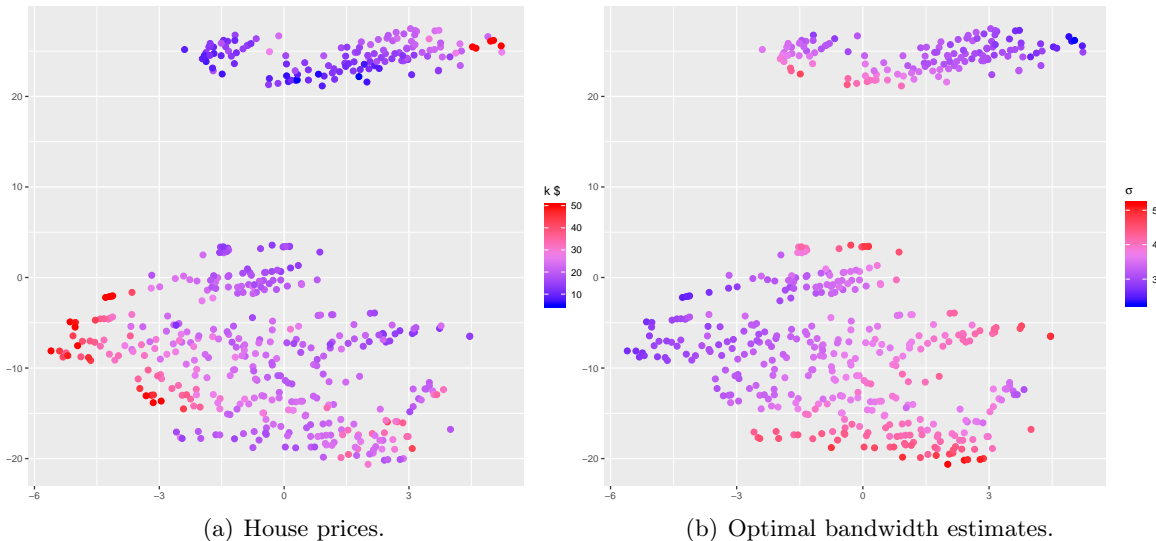


Figure 4: Properties of the Boston housing dataset plotted with respect to a 2-dimensional t-SNE embedding.

The housing price can be seen in Fig. 4 (let), accordingly. For 50 repetitions we randomly split the dataset into 306 training-, 100 validation- and 100 test-examples. Using standard GPR, we obtain an average RMSE performance of 3.05 ± 0.05 , which is significantly outperformed by KMKER with a RMSE of 2.77 ± 0.05 . Fig. 4 (right) shows the average bandwidth function. In comparison, Yuan et al. (2009) report a $\text{RMSE} = 2.84$ with a training size of 481 applying their adaptive spherical Gaussian kernel relevance vector machine approach.

5.3 Malonaldehyde Molecular Dynamics

The chemical formula of malonaldehyde is given by $C_3O_2H_4$, which structure can be seen in Fig.5. The raw inputs are the 3D-positions of the nine atoms $(R_k)_{k=1}^9$, from which we generate the reciprocal distances $\|R_k - R_l\|^{-1}$ of all atom pairings—in total 36 features—inspired by the Coulomb features. We conduct our experiments on the unrelaxed dataset from molecular dynamics (MD) simulation, while also showing our bandwidth analysis for the relaxed configurations of malonaldehyde.

Since the number of features is moderate here, we apply ARD to determine the importance of specific atom pairs, which can be seen in Fig. 6. We observe that the features describing

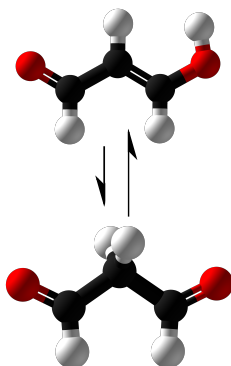


Figure 5: The Two stable states of the malonaldehyde molecule.

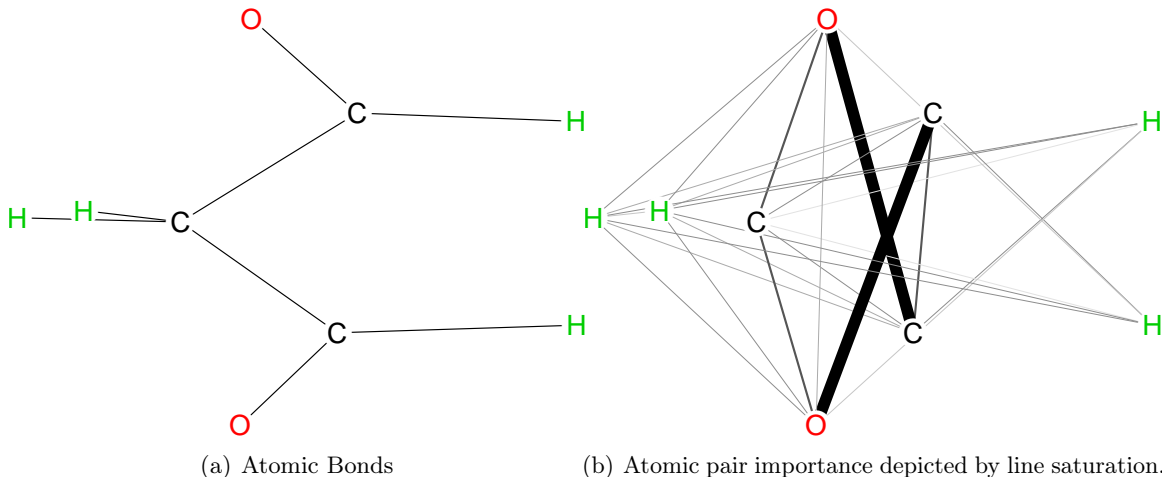


Figure 6: Exemplaric Malonaldehyde molecule conformation.

the geometry within each ‘functional group’ (that is, the outer COH ’s and the central CH_2) has negligible influence on the energy. In contrast ARD affirms the geometry of the ‘C-C-C-O’ chains to be most important which matches insights from the physical point-of-view.

For visualization purpose—and due to physical plausibility—we plot the properties of interest against the dominant *dihedral angles* of the molecule, given by the two atomic ‘C-C-C-O’ chains. The top of Fig. 7 shows the energy surface of the malonaldehyde configurations.

Table 1 show the prediction performance for the malonaldehyde MD dataset based on 5000 training samples. We observe a boost in performance when taking featurewise importance, as well as spacial inhomogeneity into account.

5.4 Atomization Energies of GDB-9

We conduct experiments on the Many-Body Descriptors for prediction of atomization energies, discussed by Pronobis et al. (2018). These describe interactions between sub-groups of two and three atoms, totalling 3270 features. The GDB-9 dataset constitute the database of all

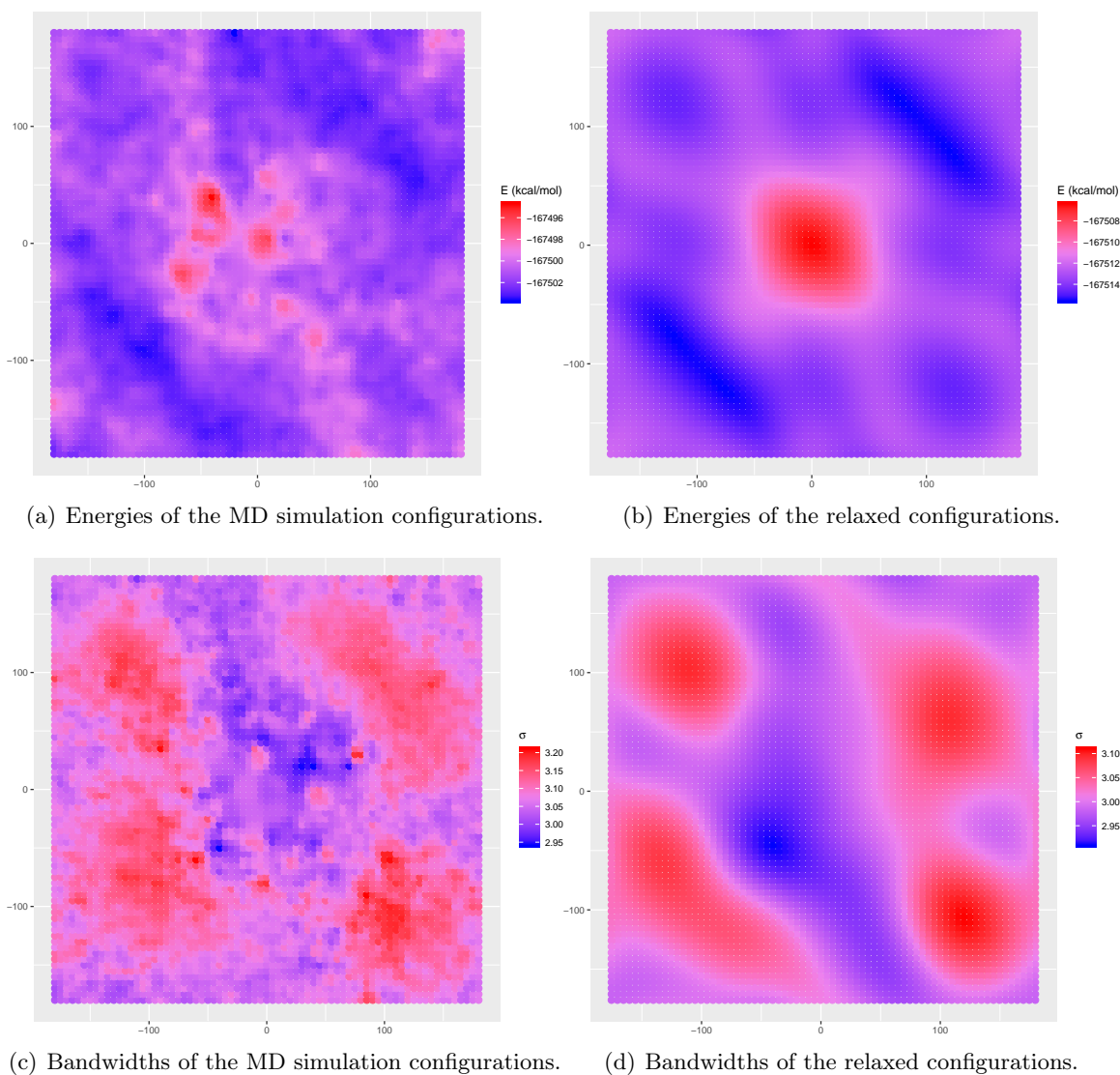


Figure 7: Surfaces are plotted with respect to the dominant dihedral angles of malonaldehyde.

stable and synthetically accessible organic molecules composed of (C,N,O,H) with up to 9 heavy atoms (C,N,O). GDB-9 is a subset of the GDB-17 (Ruddigkeit et al., 2012) database, totalling 131722 molecules.

Atomization energies of the molecules have been calculated using hybrid density functional theory at the B3LYP/6-31G(2df,p) level of quantum chemistry (Ramakrishnan et al., 2014). Fig. 8 shows the energies plotted with respect to the two leading PCA components.

We base our further analysis on 10000 training molecules. For now we apply no ARD due to the large amount of features. However, building feature subsets would be possible: We

Method	Performance		
	RMSE	MAE	max AE
GPR	0.3621	0.2611	3.3761
GPR + ARD	0.3006	0.2128	3.3009
KMKER + ARD	0.2867	0.2053	2.8755

Table 1: Results on the atomization energy prediction for the malonaldehyde MD dataset. Estimates are based on 5000 training samples.

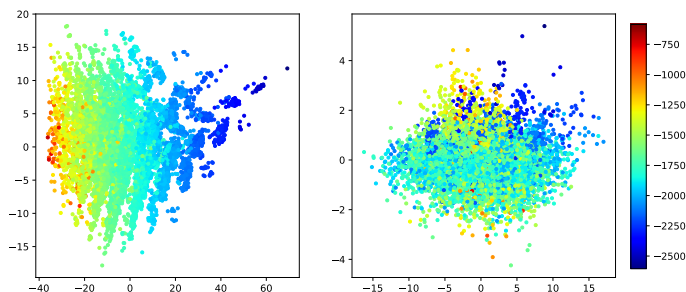


Figure 8: Atomization Energies of the GDB-9 dataset plotted with respect to PCA components. (Left) The leading PCA components. (Right) The PCA components most correlated with optimal bandwidth.

could segment the features into two groups of two-body, respectively three-body interactions. We could also segment the features into 36 groups of specific atom-combination interactions.

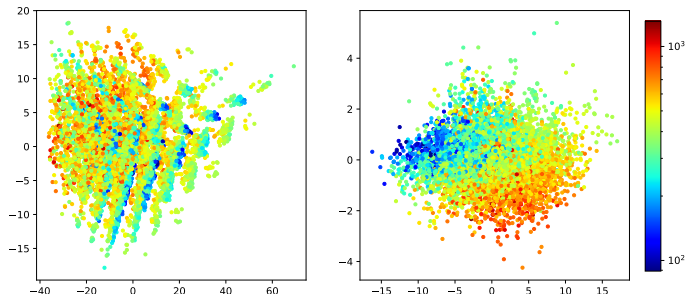


Figure 9: Optimal bandwidth of the GDB-9 dataset plotted with respect to PCA components. (Left) The leading PCA components. (Right) The PCA components most correlated with optimal bandwidth. Estimates are based on 10000 training samples.

In Fig. 9 we observe a strong pattern and quite a large spread of local bandwidth. Their meaningfulness is underpinned by an enormous performance boost, as can be seen in Table 2.

Method	Performance		
	RMSE	MAE	max AE
GPR	4.2057	1.3622	181.65
KMKER	1.8398	1.1588	35.293
relative	0.4375	0.8508	0.1943

Table 2: Results on the atomization energy prediction for the GDB-9 dataset. Estimates are based on 10000 training samples.

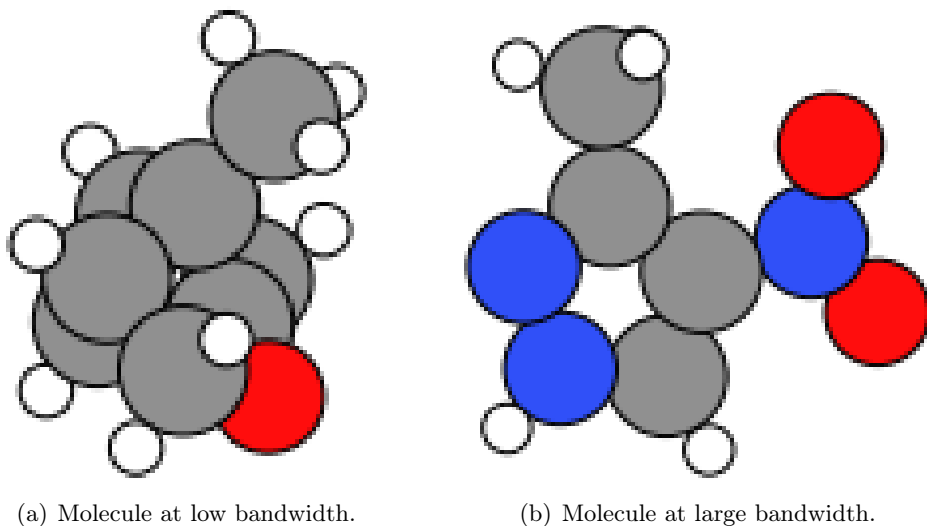


Figure 10: Exemplaric molecules for extremal bandwidth.

For a physical interpretation, we inspect the molecules which are assigned high, respectively low bandwidth. The molecules shown in Fig. 10 are prototypical: The low bandwidth molecules form clusters of carbon which we try to quantify by the total number of unique cycles contained in the molecule. On the other hand, the high bandwidth molecules contain specific chemical functional groups such as the nitro, azo and oxime group. In Fig. 11 we analyze the correlation of the number of cycles and functional groups with the local bandwidth. To the right we show the log-linear fit of these two features against the local bandwidth. Its strong agreement with the local bandwidth indicates that dense configurations of molecules antagonize functional groups in terms of complexity of energy prediction.

5.5 Thermal Cavity Flow

As an additional show case we feature a two dimensional test case from fluid mechanics, where variation of spatial resolution is often required, because of different scales present in the solution. We choose a setup that is defined by a trivial domain and simple boundary conditions, but produces a rather complex flow field. The test case is known as square cavity with differentially heated sides walls, which was first proposed for incompressible flow by De

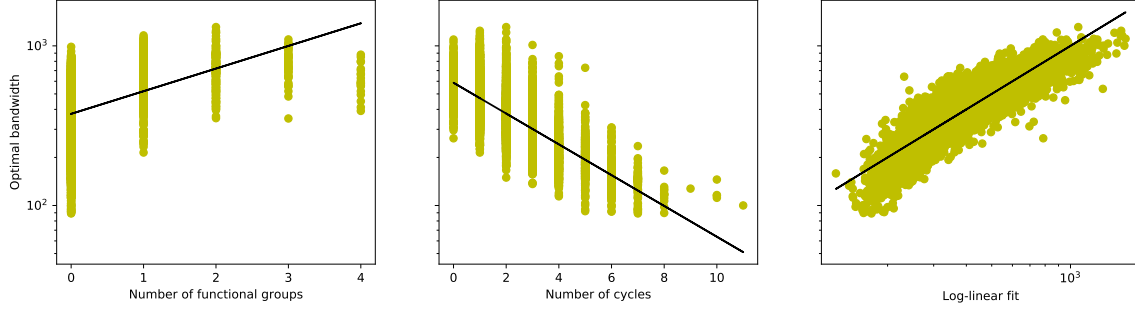


Figure 11: Correlation between the optimal bandwidth and the number of functional groups (left), the number of cycles (middle) for the GDB-9 dataset. Right: A log-linear fit of the two features (number of functional groups, number of cycles) to the optimal bandwidth.

Vahl Davis De Vahl Davis (1983) and was extended to compressible flow at large temperature differences by Vierendeels et al. (2003).

The domain is a square with four no-slip walls and subject to a gravitational potential. The top and bottom walls (w.r.t. the gravitational potential) are insulated. Left and right walls feature Diriclet boundary conditions for the temperature. The left wall is hot (i.e. T_h) and the right wall is cold (i.e. T_c). The expansion of the heated fluid and the contraction of the cooled fluid on left and right walls, respectively, will yield natural convection, i.e. rise of hot fluid and descend of cold fluid. The simulation is performed with a large temperature difference of $T_h/T_c = 4$. The most influential dimensionless number for convection flows is the Rayleigh number

$$Ra = \frac{Pr \, g \, H^3 \, (T_h - T_c)}{\nu^2} = 10^7, \quad (12)$$

where Pr is the Prandtl number, g the gravitational acceleration, H the side length of the square domain and ν the kinematic viscosity. The Rayleynumber is chosen as 10^7 , which is the highest value for which a stationary solution is reported in the reference Vierendeels et al. (2003). A visualisation of the reference flow field at this Rayleigh number based on Lenz et al. (2019b) is shown in Figure 12. Further, dimensionless numbers are the Barometric number Ba as 0.01, $Pr = 1.0$ and the number of internal degrees of freedom $K = 3$.

For the simulation a two-dimensional gas kinetic scheme (GKS) Xu (2001); Xu et al. (2005) is applied, which was previously shown to yield high quality results for thermal compressible flows and especially the square cavity with differentially heated side walls Lenz et al. (2019b). The GKS is implemented on Cartesian meshes, which are beneficial for automated mesh generation. For mesh refinement the quad tree type method proposed by Lenz et al. (2019a) is used.

The initial mesh has a uniform background resolution of 64×64 cells with two thin refinements towards the walls. These refinements are obtained when one has no prior knowledge on the flow field, apart from that the temperature and velocity gradient at the

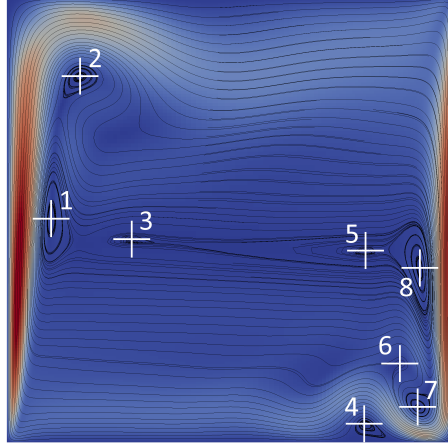


Figure 12: Reference flow field of the square cavity with differentially heated walls, based on Lenz et al. (2019b) (with permission).

wall will be large. This base line mesh contains 8608 cells. In the following process these cells are redistributed in space and over the refinement levels to improve the accuracy of the computed flow field. We alternate in a loop between the following steps:

1. Given the current mesh we run the simulation to convergence, which generates a dataset (X, y) , where the inputs X are the mesh-coordinates and y is the absolute velocity.
2. Based on (X, y) we run KMKER for 10 repetitions, randomly drawing 6000 training and 2000 validation samples, which gives us an averaged bandwidth function σ_{KMKER} .
3. With the density of X and σ_{KMKER} we propose an optimal sampling density that we discretize to take values of powers of 4 (where each power represents a refinement) and match the background resolution to not exceed the initial 8608 cells.

Note that the reorganization of grid points in Step 3 is a special case of active learning.

Figure 13 shows the evolution of the cell distribution and the corresponding velocity fields. The background resolution in the first iteration is increased to 65×65 and many cells from the fine level on top, bottom and left wall are shifted to the intermediate level. In the subsequent iteration the resolution in the background was reduced to 53×53 and both intermediate and fine level get more cells.

As a quality measure vortex centers in the velocity field are observed. The reference reports a total of eight vortices, which are also shown in Figure 12. Due to insufficient resolution the vortices 5 and 6 are not reproduced in the simulation. Here it is to note, that a resolution of about 8,600 cells is very low compared to the 40,000 cells in Lenz et al. (2019b) and 1,048,576 cells in Vierendeels et al. (2003).

The centers of the realized vortices are measured as intersection points of zero velocity contours for x - and y -velocity. The measured centers are listed in Table 3. The quality of the present simulations is evaluated in terms of Euclidean distance e of the individual vortex centers and the L2-norm e_{L2} of these e , which are both also listed in Table 3.

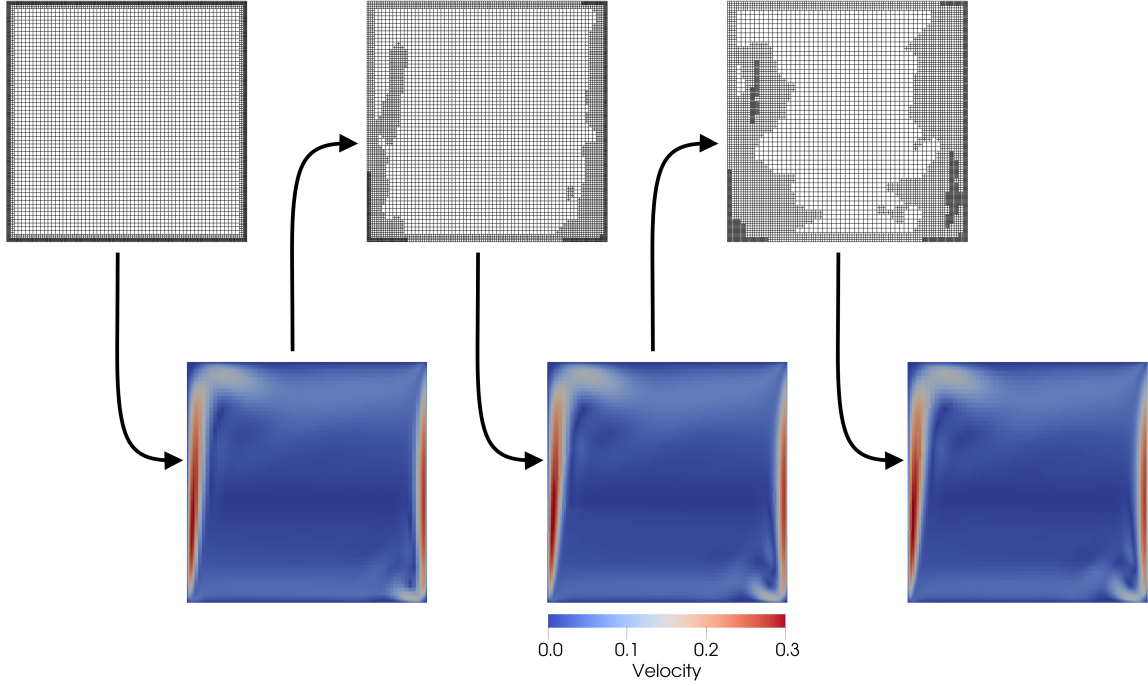


Figure 13: Mesh evolution for the square cavity with differentially heated side walls.

Observing the individual values of e shows that not all vortices improve in position in every iteration, which is probably an effect of insufficient resolution. Further the present procedure only reorganizes a given number of cells, such that no perfect solution is expected. The overall quality of the simulation can be quantified by e_{L2} . It shows, that the overall quality of the simulation increases by 32% over the two iterations. Hence, we argue that the present approach for cell redistribution improves the overall accuracy of the simulation.

However, this is just a show case. Future work on this will have to apply a more rigid analysis and a comparison to classical mesh refinement techniques that are based on local features of the flow field (e.g. gradients) or thorough error estimators.

Table 3: Vortex centers

Vortex	Reference	base line	1st iteration	2nd iteration
1	x	0.0989	0.1064	0.1001
	y	0.5016	0.4708	0.4533
	e	—	0.0317	0.0483
2	x	0.1639	0.1391	0.1491
	y	0.8211	0.7830	0.7987
	e	—	0.0455	0.0268
3	x	0.2798	0.2810	0.2751
	y	0.4556	0.4336	0.4386
	e	—	0.0220	0.0176
4	x	0.8009	0.8298	0.8324
	y	0.0419	0.0055	0.0123
	e	—	0.0465	0.0432
5	x	0.8040	—	—
	y	0.4301	—	—
	e	—	—	—
6	x	0.8807	—	—
	y	0.1765	—	—
	e	—	—	—
7	x	0.9207	0.9301	0.9228
	y	0.0793	0.0819	0.0804
	e	—	0.0098	0.0024
8	x	0.9256	0.9224	0.9244
	y	0.3909	0.3837	0.3895
	e	—	0.0079	0.0018
e_{L2}	—	0.0766	0.0724	0.0521

6. Conclusion

Locally optimal bandwidths can not only be used to raise performance of inference, but also to gain deep insights into the problem. Their estimation is a challenging meta inference task due to its indirect formulation of predicting performance of the underlying task. Additionally, the estimation of a bandwidth-function is prone to overfitting. In this work we proposed a novel local bandwidth model with strong restrictions on the degrees of freedom, which makes this approach robust. In our experiments we have shown its superior performance as well as its capabilities to be applied in data interpretation and active learning.

Future work will include an extensive study on adaptive grid selection in numerical simulations, i.e. showing convergence of the grid adaption procedure. We will also elaborate more interpretation in quantum chemistry. Finally we will try to make this approach scalable by redesigning it as a deep neural network.

Acknowledgements

The authors would like to thank Stephan Lenz and Martin Geier from the Institute for computational modeling in civil engineering of the Technische Universität Braunschweig for the fruitful discussion and active help with the simulations of the thermal cavity flow experiment.

D. Panknin and T. B. Bui were funded by the Federal Ministry of Education and Research (BMBF) under the project ALICE II, Autonomous Learning in Complex Environments (01IB15001B). D. Panknin was also funded by the BMBF project ALICE III, Autonomous Learning in Complex Environments (01IS18049B) and T. B. Bui was also funded by the BMBF project AIAx, Machine Learning-driven Engineering – CAx goes AIAx (01IS18048B). S. Nakajima was funded by the BMBF project BBDC II, Berlin Big Data Center (01IS18025A). K.-R. Müller was supported by Institute for Information & Communications Technology Promotion and funded by the Korea government (MSIT) (No. 2017-0-00451, No. 2017-0-01779).

References

- Gavin C. Cawley, Nicola L. C. Talbot, and Olivier Chapelle. Estimating predictive variances with kernel ridge regression. In *Machine Learning Challenges. Evaluating Predictive Uncertainty, Visual Object Classification, and Recognising Textual Entailment*, pages 56–77, Berlin, Heidelberg, 2006. Springer Berlin Heidelberg. ISBN 978-3-540-33428-6.
- Ziyi Chen, Jinwen Ma, and Yatong Zhou. A precise hard-cut em algorithm for mixtures of gaussian processes. In *International Conference on Intelligent Computing*, pages 68–75. Springer, 2014.
- G. De Vahl Davis. Natural convection of air in a square cavity: A bench mark numerical solution. *International Journal for Numerical Methods in Fluids*, 3(3):249–264, 1983. doi: 10.1002/flid.1650030305. URL <https://onlinelibrary.wiley.com/doi/abs/10.1002/flid.1650030305>.
- Jianqing Fan and Irene Gijbels. Variable bandwidth and local linear regression smoothers. *The Annals of Statistics*, pages 2008–2036, 1992.
- Stefano Ferrari, Francesco Bellocchio, Vincenzo Piuri, and N Alberto Borghese. Multi-scale support vector regression. In *Neural Networks (IJCNN), The 2010 International Joint Conference on*, pages 1–7. IEEE, 2010.
- Mehmet Gönen and Ethem Alpaydin. Localized multiple kernel regression. In *Pattern Recognition (ICPR), 2010 20th International Conference on*, pages 1425–1428. IEEE, 2010.
- Mehmet Gönen and Ethem Alpaydın. Multiple kernel learning algorithms. *Journal of machine learning research*, 12(Jul):2211–2268, 2011.
- Vincent Guigue, Alain Rakotomamonjy, and Stéphane Canu. Kernel basis pursuit. In *European Conference on Machine Learning*, pages 146–157. Springer, 2005.

- David Harrison and Daniel L Rubinfeld. Hedonic housing prices and the demand for clean air. *Journal of Environmental Economics and Management*, 5(1):81 – 102, 1978.
- Kristian Kersting, Christian Plagemann, Patrick Pfaff, and Wolfram Burgard. Most likely heteroscedastic gaussian process regression. In *International Conference on Machine Learning (ICML)*, 2007.
- Stephan Lenz, Martin Geier, and Manfred Krafczyk. An explicit gas kinetic scheme algorithm on non-uniform cartesian meshes for gpgpu architectures. *submitted to Computers & Fluids*, 2019a.
- Stephan Lenz, Manfred Krafczyk, Martin Geier, Songze Chen, and Zhaoli Guo. Validation of a two-dimensional gas-kinetic scheme for compressible natural convection on structured and unstructured meshes. *International Journal of Thermal Sciences*, 136:299–315, 2019b. ISSN 12900729. doi: 10.1016/j.ijthermalsci.2018.10.004.
- Laurens van der Maaten and Geoffrey Hinton. Visualizing data using t-sne. *Journal of Machine Learning Research*, 9(Nov):2579–2605, 2008.
- Edward Meeds and Simon Osindero. An alternative infinite mixture of gaussian process experts. In *Advances in Neural Information Processing Systems*, pages 883–890, 2006.
- Wiktor Pronobis, Alexandre Tkatchenko, and Klaus-Robert Müller. Many-body descriptors for predicting molecular properties with machine learning: Analysis of pairwise and three-body interactions in molecules. *Journal of Chemical Theory and Computation*, 14(6): 2991–3003, 2018.
- Raghunathan Ramakrishnan, Pavlo O Dral, Matthias Rupp, and O Anatole Von Lilienfeld. Quantum chemistry structures and properties of 134 kilo molecules. *Scientific data*, 1: 140022, 2014.
- Lars Ruddigkeit, Ruud van Deursen, Lorenz C. Blum, and Jean-Louis Reymond. Enumeration of 166 billion organic small molecules in the chemical universe database gdb-17. *Journal of Chemical Information and Modeling*, 52(11):2864–2875, 2012.
- Volker Tresp. Mixtures of gaussian processes. In *Advances in neural information processing systems*, pages 654–660, 2001.
- Jan Vierendeels, Bart Merci, and Erik Dick. Benchmark solutions for the natural convective heat transfer problem in a square cavity with large horizontal temperature differences. *International Journal of Numerical Methods for Heat & Fluid Flow*, 13(8):1057–1078, 2003. ISSN 0961-5539. doi: 10.1108/09615530310501957.
- Christian Walder, Kwang In Kim, and Bernhard Schölkopf. Sparse multiscale gaussian process regression. In *Proceedings of the 25th International Conference on Machine Learning, ICML ’08*, pages 1112–1119, New York, NY, USA, 2008. ACM.
- Kun Xu. A Gas-Kinetic BGK Scheme for the Navier–Stokes Equations and Its Connection with Artificial Dissipation and Godunov Method. *Journal of Computational Physics*, 171(1):289–335, 2001. ISSN 00219991. doi: 10.1006/jcph.2001.6790.

- Kun Xu, Meiliang Mao, and Lei Tang. A multidimensional gas-kinetic BGK scheme for hypersonic viscous flow. *Journal of Computational Physics*, 203(2):405–421, 2005. ISSN 00219991. doi: 10.1016/j.jcp.2004.09.001.
- Yan Yang and Jinwen Ma. An efficient em approach to parameter learning of the mixture of gaussian processes. In *International Symposium on Neural Networks*, pages 165–174. Springer, 2011.
- Azhong Ye, Rob J Hyndman, and Zinai Li. Local linear multivariate regression with variable bandwidth in the presence of heteroscedasticity, 2006.
- Chao Yuan and Claus Neubauer. Variational mixture of gaussian process experts. In *Advances in Neural Information Processing Systems*, pages 1897–1904, 2009.
- Jin Yuan, Liefeng Bo, Kesheng Wang, and Tao Yu. Adaptive spherical gaussian kernel in sparse bayesian learning framework for nonlinear regression. *Expert Systems with Applications*, 36(2):3982–3989, 2009.
- Seniha Esen Yuksel, Joseph N Wilson, and Paul D Gader. Twenty years of mixture of experts. *IEEE transactions on neural networks and learning systems*, 23(8):1177–1193, 2012.
- Danian Zheng, Jiaxin Wang, and Yannan Zhao. Non-flat function estimation with a multi-scale support vector regression. *Neurocomputing*, 70(1):420–429, 2006.

Appendix A. The local linear smoother

Let

$$\hat{f}(z) = \alpha_{\sigma,x} + \beta_{\sigma,x}^\top(z - x)$$

be a linear expansion with focus in x and hyperparameters $\alpha_{\sigma,x}, \beta_{\sigma,x} \in \mathbb{R}$. Estimates for the hyperparameters can be found by solving the *local least squares problem* in x :

$$\sum_{i=1}^n (y_i - \alpha_{\sigma,x} - \beta_{\sigma,x}^\top(x_i - x))^2 k^\sigma(x, x_i)$$

Then the local linear smoother is given by

$$m^\sigma(x) = \alpha_{\sigma,x},$$

where σ is a free parameter. Therefore there exists an optimal $\sigma(x)$ -choice for predicting the label of x based on $m^{\sigma(x)}$.